Structural transition in chiral nematic liquid crystal droplets in an electric field

J. Bajc and S. Žumer
Department of Physics, University of Ljubljana, Jadranska 19, 1000 Ljubljana, Slovenia
(Received 23 September 1996)

Director fields in droplets of chiral nematic (cholesteric) liquid crystals with negative dielectric anisotropy exposed to an electric field are modeled. Field induced continuous transitions from low-field structures with spherical chiral nematic surfaces to high-field structures with planar chiral nematic surfaces via intermediate structures with oblate chiral surfaces are discussed. Depending on initial spherical structures, three possible transitions are analyzed. Numerically modeled evolution of the intermediate structures, obtained by the free-energy considerations and model director fields, agrees very well with the published observations by Crooker and co-workers. [S1063-651X(97)00603-X]

PACS number(s): 64.70.Md, 61.30.Cz, 61.30.Jf

I. INTRODUCTION

Confined chiral nematic (N^*) liquid crystals are the subject of many recent investigations [1–4], since they are interesting from practical and basic aspects [5–7]. The structure of a nematic liquid crystal is completely characterized by the nematic director field $\vec{n}(\vec{r})$ with the equivalence of the $\vec{n}$ and $-\vec{n}$ state. However, it is often practical to describe the structure of the N^* phase with the twist field $\vec{q}(\vec{r})$ that points in the direction of the axis characterizing local twist of the director field $\vec{n}(\vec{r})$ [8]. Clearly $\vec{n}(\vec{r})$ would suffice, but the field $\vec{q}(\vec{r})$, although carrying less information, is sometimes more illustrative. In such a case the term ''chiral nematic (N^*) surface'' is introduced for the surface normal to $\vec{q}(\vec{r})$. The director is thus everywhere tangential to the N^* surface.

The subject of the paper is a droplet of chiral nematic liquid crystal in an electric field [3,9]. Confinement deforms the homogeneous twist field $\vec{q} \neq \vec{q}(\vec{r})$ of the unconstrained N^* phase. The structure of a droplet is a result of a competition between field and surface effects. Due to negative dielectric anisotropy the director tends to be perpendicular to the applied electric field—the field aligns $\vec{q}$ parallel to $\vec{E}$. On the other hand, the confinement to a spherical cavity and parallel anchoring on the cavity wall forces N^* surfaces to be as spherical as possible to minimize the total surface free energy. Thus in the absence of the field the structures with spherical N^* surfaces are the most stable ones. In a high enough electric field the spherical structures transform into planar ones. Experimental studies of droplets with diameter between 10 and 40 μm showed that this transition is continuous [3]. Intermediate structures are characterized by a flat central region in which the field $\vec{q}(\vec{r})$ is already aligned with the electric field and an outer region in which the N^* surfaces still preserve curved shape due to degenerate parallel anchoring at the cavity wall. The flat central region appears when the field crosses a certain threshold value. Its size depends on the strength of the field [3]. The authors report that the growth of the central region with the field is not entirely continuous—a steplike behavior is observed.

In our previous paper, these intermediate structures were modeled merely from the topological point of view [9]. Then a crude estimate, based on the length and strength of disclination lines, was used to calculate the total free energy of the structures. The qualitative agreement with the experiments was good, although the threshold values were overestimated and a steplike behavior of the growth of the flat central region of the droplet was not explained. In the present paper models for the director fields of the intermediate structures, which give a better estimate of the total free energies of intermediate structures, are constructed. The calculated threshold values of the transition are now much closer to the observed ones and the steplike behavior can also be explained.

In Sec. II the improved model of the intermediate structures is described in detail and briefly compared with the previous model. In Sec. III the free energies and transitions are calculated. Finally, the results are discussed in Sec. IV.

II. MODELING OF CHIRAL STRUCTURES

In order to describe the intermediate structures, an intuitive analytical model based on rotational ellipsoidal N^* surfaces was used in our previous paper [9]. At the time the models for the director field of initial spherical and final planar structures were known [10,11], but the models for the director field of the intermediate structures have been developed only recently and are presented here. Calculations were therefore based on a simple mathematical model for N^* surfaces—rotational ellipsoids. Furthermore, infinitely strong degenerate parallel anchoring was assumed to make the topological description easier and the elastic free energy was ascribed to the defect lines according to their length and strength. The description of the defect lines is well defined by the topological constraints and is mathematically simple at all stages of the transition. Depending on the initial spherical structure and its orientation in the electric field four possible intermediate structures were predicted. Later it turned out that the radial defect line oriented parallel to the applied field is not metastable as supposed, but unstable, so in fact there are only three possible intermediate structures. In an electric field spherical N^* surfaces deform into oblate rota-

tional ellipsoids, which have the same shape for all intermediate structures: let their short axis be denoted d and the other two $d+\delta$. Clearly, $\delta=0$ corresponds to spherical and $\delta\rightarrow\infty$ to planar structures, and the transition can be described by the dependence of δ, the eccentricity parameter of the N^* surfaces, on the electric field.

If the N^* surfaces are known, the length of the defect lines for the structures can be calculated and the elastic free energy can be estimated. The electric free energy can only be estimated for high chirality ($qR \gg 2\pi$) (R is the droplet radius), when the average of the electric free energy density over one pitch can be calculated. This average electric free energy can be represented as a function of the field $\vec{q}(\vec{r})$, rather than a function of the field $\vec{n}(\vec{r})$. In this frame the analytic expression for the free energy was derived in the one elastic constant approximation. The results give reasonable qualitative matching with the experiments, but the quantitative matching is not so satisfactory. As discussed in [9] there are several reasons for the lack of a quantitative matching: the assumption of infinite anchoring being the first to question.

The infinite anchoring approximation is usually justified with large size of the system. It is known that the strength of an interaction can be expressed with a particular length. These characteristic lengths measure distances, where the changes of the ordering, induced by a particular effect, become significant. Examples of such lengths are the electric $\xi_E=\sqrt{K/(\varepsilon_0|\varepsilon_a|E^2)}$ and magnetic $\xi_B=\sqrt{K\mu_0/(|\chi_a|B^2)}$ coherence lengths, the surface extrapolation length $d_s=K/W_0$, etc. Shorter length means stronger interaction. On this basis, for a nematic system, the anchoring is said to be strong, if $d_s \ll D$, where D is a characteristic dimension of the system (for the sphere $D=R$). In chiral systems another length—pitch—is relevant. In order to state what sort of anchoring one has, d_s must now be compared to both the radius R and pitch $\mathcal{P}=2\pi/q$.

A simple calculation in cylindrical geometry illustrates the above considerations and gives an idea of the meaning of the symbol ''$\ll$'' when comparing characteristic lengths. Suppose that $\vec{q}$ is parallel to the cylinder axis so that the structure in the whole cylinder is obtained by rotating the structure on a particular N^* surface (a disk) by qz when moving a distance z along the axis of the cylinder. In the case of infinite anchoring and high chirality limit the director field on the N^* surface is almost uniform. It deviates only in the vicinity of the surface in order to satisfy the infinite anchoring. Let us estimate the thickness of this region. The rotation of $\vec{n}$ by an angle $\gamma \leqslant \pi/2$ is needed to adjust the director to the surface. The thickness of the nonuniform region can thus be estimated as $\mathcal{P}/4=\pi/2q$. The corresponding elastic free energy on account of the unwound N^* phase is

$$F_{\text{strong}}=\frac{1}{2}\frac{K_{22}}{2}q^2\frac{\pi}{2q}2\pi RL=\frac{1}{2}K_{22}qR\pi^2L, \tag{1}$$

where the averaging of the twist energy over the region yields $\frac{1}{2}$, K_{22} is the twist elastic constant, and L is the length of the cylinder. The surface contribution to the free energy is zero due to infinite anchoring. In fact, F_{strong} is even larger due to splay and bend contributions to the total elastic free energy [8].

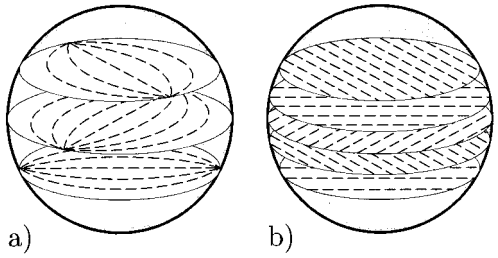

FIG. 1. Schematic presentation of the director field in planar structures: (a) infinitely strong and (b) zero parallel anchoring. For the case of infinite parallel anchoring (a) corresponds to relatively small chirality $qR \lesssim 1$. With increasing chirality the director field on each circular N^* surface looks more and more uniform. When $qR \gtrsim 100$ the director field is uniform on most of the circle except for a thin stripe at the border of the circle. The director field thus looks like the one for the zero anchoring (b), implicitly indicating that a pitch much smaller than the surface extrapolation length $d_s=K/W_0$ results in the weak anchoring regime.

The other limiting case is the one with completely uniform director field on each circle. In this case the elastic free energy is zero due to completely satisfied twist, but the surface free energy is nonvanishing. If the surface free energy of the Rapini-Papoular [12] form is supposed,

$$F_s=\tfrac{1}{2}W_0\oint_S \sin^2\Theta\, dS, \tag{2}$$

where Θ is the angle between the preferred and the actual director orientation and W_0 is the surface anchoring strength, the total free energy becomes

$$F_{\text{uniform}}=\tfrac{1}{2}RW_0\pi L. \tag{3}$$

Clearly, F_{uniform} is the upper limit for the total free energy in the finite anchoring regime. If the infinite anchoring is to be considered as a possible approximation the total free energy F_{strong} must inevitably be less than F_{uniform} or equivalently the surface extrapolation length must be less than a few hundredths of a pitch $\mathcal{P}$,

$$\frac{K_{22}}{W_0}=d_s<\frac{1}{2\pi^2}\mathcal{P}\sim 0.05\mathcal{P}. \tag{4}$$

In the one constant approximation, the values $K=5\times10^{-12}$ N and $W_0=0.2$ mJ/m^2 [8,13,14] give the surface extrapolation length $d_s=25$ nm, making the infinite anchoring approximation questionable for $\mathcal{P}<500$ nm. Figure 1 illustrates the above limiting possibilities in the case of spherical confinement. In Fig. 1(a) the director field of the planar bipolar structure is shown for the infinite parallel anchoring. Note that the point defects on successive circles form a double surface χ defect spiral, which becomes very long (compared to the droplet radius R) for a highly chiral N^* phase. In Fig. 1(b) the director field in the droplet for the case of a uniform director arrangement on each circle is sketched. The estimated free energy for the structure shown in Fig. 1(a) is almost $1400\pi KR$ for $R=10$ μm,

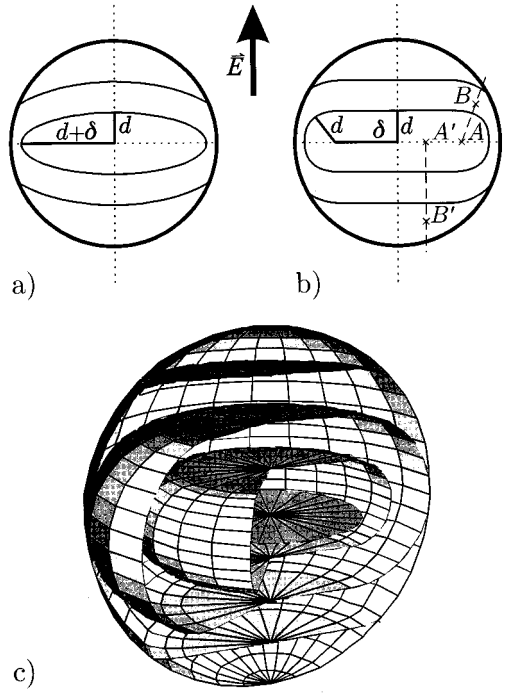

FIG. 2. Schematic presentation of the chiral nematic surfaces in the (a) previous (topological) and (b) and (c) improved models. For $d+\delta<R$ chiral nematic surfaces are closed, whereas for $d+\delta>R$ chiral nematic surfaces are cut in two parts. In the previous model the infinite anchoring forces the director $\vec{n}(\vec{r})$ to be tangential to the border of the cut chiral nematic surface, resulting in additional defects. In the improved model no deformation of the director field due to the presence of the surface is taken into account, so all chiral nematic surfaces are topologically equivalent to a sphere. In the construction of the director field in the droplet use is made of the fact that each point in the droplet (for example, B or B') corresponds to precisely one point on the central circle (in this case A and A'). The connection between the points is determined by the field of helical axes $\vec{q}(\vec{r})$. See the text for details.

$\mathcal{P}=500$ nm, and the above cited values for K and W_0, whereas for the structure shown in Fig. 1(b) the free energy is approximately $270\pi KR$, which makes this structure energetically more favorable.

The next reason for the quantitative failure of the previous model is nonconstant pitch. Taking oblate rotational ellipsoids as the ansatz for the N^* surfaces results in large spatial variation of $|\vec{q}|$, especially in the vicinity of the equatorial plane. On the other hand, the observed difference between actual and intrinsic pitch is very small in the bulk as well as in confined systems [15]. In order to limit the spatial variation of $|\vec{q}|$, equidistant N^* surfaces are constructed in the improved model.

A. Improved model

In the spirit of the above considerations an improved model of the intermediate structures is proposed. The construction is based on the following facts.

The chiral nematic surfaces of the intermediate structures are built up of two concentric disks of radius δ separated by $2d$, and the outer part of a torus with the radius of its center equal to δ and the radius of its tube equal to d. Equivalently,

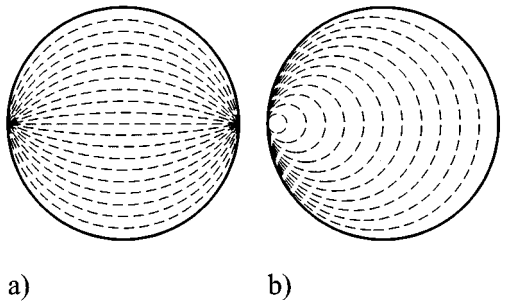

FIG. 3. Director field on a circle with infinite parallel anchoring at the circle edge. (a) Bipolar structure with two $s'=1$ surface point defects and (b) monopolar structure with one $s'=2$ surface point defect. If the defects are treated as bulk instead of surface type defects, then their strengths should be halved. The bipolar structure therefore has two $s=\frac{1}{2}$ bulk point defects and the monopolar structure has one $s=1$ bulk point defect. All the defects lie very close to the border in order to minimize the free energy.

the shape of an N^* surface is the same as the shape of an elastic membrane stretched over a torus (see Fig. 2). The center of each N^* surface remains in the center of the droplet and the two disks are perpendicular to the applied electric field. With such an ansatz, the distance between the successive N^* surfaces is kept constant. When $\delta=0$ the structures are spherical and $\delta\geqslant R$ corresponds to planar structures which appear in high electric field. It is convenient to normalize δ with respect to R, which is to define $\epsilon\equiv\delta/R$. When the size of a particular N^* surface is too large (i.e., $d+\delta>R$), the droplet surface cuts it into two parts, but the shape of these two parts is not altered.

The director field for the intermediate structures $(0<\delta\leqslant R)$ is constructed from the ansatz for the director field on the central circle (radius δ), known pitch, and the fact that the axis of rotation in the N^* phase lies normal to the N^* surfaces. Possible director configurations on the central circle are deduced from the known director at its boundary (radius equal to δ)—it must be tangential to it, since the director is supposed to be tangential to the N^* surfaces, and the boundary of the circle is a line [16]. In the case of infinitely strong anchoring there are two topologically different cases: the N^* surfaces are either closed (equivalent to a sphere) or cut by the droplet surface into two parts (each equivalent to a circle). The director field in the case of the improved model, on the other hand, does not change in the vicinity of the droplet surface and each N^* surface is topologically equivalent to a sphere. The only difference between the director fields on particular N^* surfaces is that some lie entirely in the droplet and some are partially cut off by the droplet surface. Particular cases are discussed later.

The field of helical axes consists of straight lines due to equidistant N^* surfaces. Therefore $|\vec{q}|$ is closer to the intrinsic q than in the previous model. Nevertheless, even when the director field of an oblate structure is constructed in such a way that any two directors lying a distance l apart along a helical axis are relatively rotated for the angle lq, i.e., the intrinsic twist seems to be satisfied in the entire droplet, the twist free energy contribution in the toroidal part of the droplet is not zero. This is a consequence of the λ defect line at the border of the central circle. A similar structure is found in

cylindrical cavities, and is known as the radially twisted or double twisted structure [15,17,18]. The structure has a λ line along the tube axis [z axis in cylindrical coordinate system, see Fig. 11(a)]. The director is parallel to the tube axis in the center of the tube, and is rotating about $\vec{e}_\rho$ in the rest of the tube, for example, $\vec{n}=\cos(qr)\vec{e}_z-\sin(qr)\vec{e}_\phi$. The local helical axes are $\vec{q}_1=\vec{e}_\rho$ and $\vec{q}_2=\cos(qr)\vec{e}_\phi+\sin(qr)\vec{e}_z$. The analysis of the local director with the twist pseudotensor, first introduced by Kilian and Sonnet [19], confirms the double twist character of the director field in the toroidal part of the droplet. The shape of the N^* surfaces results in the following general director field in the toroidal part of the droplet [expressed in toroidal coordinates, see Appendix and Fig. 11(b)]:

$$\vec{n}=\cos[\Omega(r,\theta,\phi)]\vec{e}_\theta+\sin[\Omega(r,\theta,\phi)]\vec{e}_\phi . \tag{5}$$

Locally the director rotates about two twist axes with the corresponding wave numbers:

$$q_1=\frac{\partial\Omega}{\partial r},\quad q_2=-\frac{\delta\,\sin(2\Omega)}{2r(\delta+r\,\sin\theta)}. \tag{6}$$

The first axis of rotation is, as expected, $\vec{e}_r$, whereas the second one is far less obvious and reads

$$\left[r\,\cos\Omega\left(\cos\Omega+\frac{\partial\Omega}{\partial\phi}\right)-(e+r\,\sin\theta)\,\sin\Omega\,\frac{\partial\Omega}{\partial\theta}\right]\vec{e}_r$$
$$+\sin\Omega\left[\frac{e\,\sin(2\Omega)}{2}+r\,\frac{\partial\Omega}{\partial r}(e+r\,\sin\theta)\right]\vec{e}_\theta$$
$$-\cos\Omega\left[\frac{e\,\sin(2\Omega)}{2}+r\,\frac{\partial\Omega}{\partial r}(e+r\,\sin\theta)\right]\vec{e}_\phi .$$

The second wave number equals zero, if the structure is spherical (i.e., $\delta=0$) or if $\Omega(\vec{r})=N\pi/2$ (where N is an integer) which does not result in the chiral structures that are required. It follows that the twist free energy of oblate structures cannot be zero.

At the droplet surface degenerate planar anchoring is assumed. Its strength is supposed to be finite, but still rather strong as in the experimental studies by Crooker and coworkers [1–3]. In order to keep the calculations as simple as possible, the director field close to the droplet surface is determined the same way as in the central parts of the droplet and is not adjusted to fulfill the boundary conditions. In reality the director field near the surface is deformed in order to minimize the total free energy. Since these adjustments are difficult to include in the type of calculations performed here, no deviations of the director field at the surface are taken into account. The surface free energy is thus simply added to the total free energy.

The total free energy of a particular structure is calculated in the following way. The free energy density is derived analytically using the known director field. Then the integration of the free energy density is performed numerically. It consists of the integral over the volume of the droplet for elastic and field contribution and of the integral over the droplet surface for the interfacial contribution. The elastic free energy is a sum of splay, twist, bend, and core contribution that are calculated separately so that the one elastic constant approximation is no longer essential.

B. Oblate structures

Saying that a transition from a particular spherical to a particular planar structure is continuous means that the director field changes continuously. The modeled intermediate oblate structure, characterized with $\epsilon\equiv\delta/R$, must therefore be chosen so as to continuously connect the particular initial spherical structure with the particular final planar structure. In other words, the intermediate oblate structure must yield the initial spherical structure for $\epsilon=0$ and the specific planar structure for $\epsilon\geqslant 1$. The first impression is that the transition is complete when $\epsilon=1$. It is true that $\epsilon=1$ defines a planar structure, but it is not necessarily the desired final planar structure—it does not necessarily have minimal total free energy.

The first step in the transition is the change from a spherical ($\epsilon=0$) to an intermediate oblate structure ($\epsilon>0$). This transition is accompanied by the creation of the circle with radius $\delta=\epsilon R$ in the center of the droplet. The director field on this circle is used later as the ''cornerstone'' of the director field in the entire droplet. In order to obtain possible director fields on the central circle the boundary conditions at its circumference must be determined. Since the circle lies in the bulk N^* phase, the boundary conditions are not immediately obvious. Taking the assumption of oblate N^* surfaces to be valid in the entire droplet, the central circle can be viewed as the oblate N^* surface with short axis $d=0$ and long axes $d+\delta=\delta$. Demanding $\vec{n}(\vec{r})$ to be tangential to the N^* surface is thus equivalent to infinitely strong tangential anchoring at the circle edge. This is the same as saying that the borderline of the circle is a λ line, where the $\vec{q}(\vec{r})$ field is singular and the $\vec{n}(\vec{r})$ field is not [8]. The allowed director fields for a two-dimensional nematic bound to a circle are well known, the most stable being the so-called monopolar and bipolar structure [16] (Fig. 3).

Since no observations of discontinuous transitions between different intermediate structures have been published, those transitions are not taken into account in the forthcoming calculations. This implies that the transition is described by the initial spherical structure and appropriate intermediate oblate structure which changes its shape, depending on the applied field. A description of such a transition is sufficiently described by the function $\epsilon(E)$, which is yet to be calculated.

1. Construction of the director field

Once the director field on the central circle is determined, the director in the rest of the droplet can be calculated. The field of helical axes consists of straight lines attached to the central circle and pointing outwards. For each point B in the droplet there is precisely one point A on the central circle such that a straight line along $\vec{q}(\vec{r})$ connects them ($\vec{q}_{AB}\|\overrightarrow{AB}$). The distance between the points determines the angle of rotation: $\alpha=\vec{q}_{AB}\cdot\overrightarrow{AB}$ [see Fig. 2(b)]. Such a director field satisfies the intrinsic twist along $\vec{q}(\vec{r})$ in the entire droplet. However, double twist cannot be avoided in the toroidal part of the droplet. Since it is not possible to satisfy the intrinsic twist in both directions, the twist contribution to

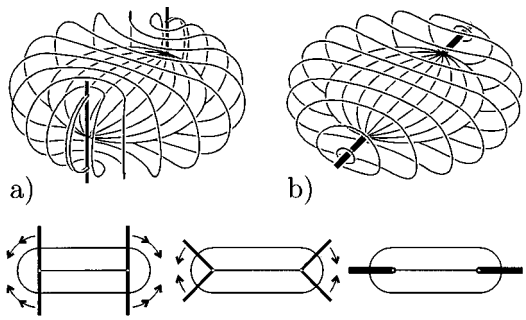

FIG. 4. Topological transformation of the parallel diametrical oblate structure into the normal diametrical oblate structure. Top: the three-dimensional director fields on two typical chiral nematic surfaces [the (a) parallel diametrical oblate structure and (b) normal diametrical oblate structure]. The transformation is illustrated by cross sections of chiral nematic surfaces and χ lines (bottom). The two $s=\frac{1}{2}$ χ lines are broken at the border of the central circle. Then each half of the χ line is rotated by 90° into the plane of the central circle. The rotated $s=\frac{1}{2}$ χ lines fuse into one $s=1$ χ line. The thickness of a defect line corresponds to its strength. For details about both diametrical oblate structures see Sec. II C.

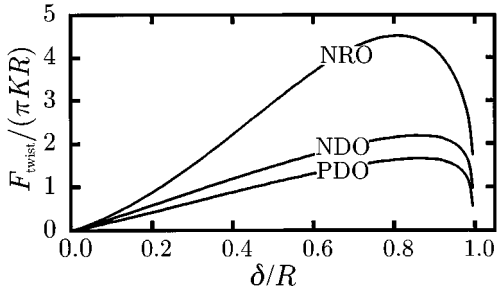

FIG. 5. Influence of stretching on the twist free energy. Stretching of the director field of the parallel diametrical oblate (PDO) structure results in the normal diametrical oblate (NDO) structure. The corresponding twist free energy is increased due to unsatisfied intrinsic twist along $\vec{q}(\vec{r})$, but the increase is relatively small during the entire transition $0<\epsilon=\delta/R<1$. For comparison, the twist contribution of the normal radial oblate (NRO) structure is added. Note that the twist free energy of the NRO structure is approximately twice the twist free energy of the NDO structure. The same is true for the bend, splay, and core free energies. See Sec. III for details.

the free energy is not identically zero. The application of the above rule has the very important consequence that χ defect lines are normal to the N^* surfaces. A further consequence is a condition that the χ lines in oblate structures must be normal to the central circle, since they originate from point defects on it. The resulting director field does not allow the defect lines in the plane of the central circle. On the other hand, defect lines in all experimentally observed oblate structures lie perpendicular to the applied electric field, i.e., they lie in the plane of the central circle.

Therefore a slight modification of the above director field is made. The modification has to be such that defect lines, parallel to the field (i.e., normal to the central circle), are rotated for 90° to be in the plane of the central circle. In other words, the director field above and below the central circle should somehow be expanded to the rest of the droplet. An example of such a transformation is given in Fig. 4. Representing an N^* surface with an elastic surface—this is due to elasticity of the nematic liquid crystals—one can imagine a stretching of the director structure on a circle above (or below) the central circle over the toroidal part of the same N^* surface to its equator. Taking the stretching factor to be constant for the entire N^* surface makes it possible to describe the process in a mathematical language. The director field above and below the central circle is calculated as before, taking $\vec{q}(\vec{r})$ parallel to the z axis, which points along the electric field $\vec{E}$. The director field, calculated this way at a certain point $\vec{r}_1$, has to be moved to a point $\vec{r}_2$, according to the stretching factor

$$\frac{\delta+\pi d/2}{\delta}=1+\frac{\pi d}{2\delta}, \tag{7}$$

where δ is the central circle radius and d the distance between a particular N^* surface and the central circle. For $d=0$ no stretching is needed, because the N^* surface does not have a toroidal part, and more and more stretching is needed as d is increased and there is more of a toroidal part to which the director field has to be stretched. The stretching factor, defined this way, rotates parallel defect lines (parallel to the applied electric field $\vec{E}$) for 90° into the normal defect lines (Fig. 4). The intrinsic twist along $\vec{q}(\vec{r})$ is no longer fulfilled in the entire droplet, but the calculations show that the twist free energy is still close to the one obtained for the nonstretched structure (see Fig. 5).

By choosing an appropriate director configuration on the central circle and applying one of the above methods, oblate structures with χ lines perpendicular or parallel to the applied electric field can be modeled. Only perpendicular χ lines were observed in oblate structures and only perpendicular or parallel orientation of χ lines in spherical structures in low electric field was found to be stable [9]. Therefore modeled director fields of intermediate structures represent a sufficient set to describe all possible transitions from spherical to planar structures.

At this point it should be stressed that as far as defect lines are concerned there is a very important difference between the previous and the improved model. For the previous model, the infinitely strong parallel anchoring resulted in topological equivalence of the cutoff part of the N^* surface with a circle and further to the formation of point defects at the edge of the cutoff N^* surface. These point defects form long surface χ lines which increase the elastic free energy a lot. On the other hand, in the improved model the surface defect lines are removed because the anchoring is no longer infinitely strong.

C. Particular cases

To get planar structures from spherical ones, there are several possibilities, depending on the initial spherical structure and its orientation in electric field. There are three spherical structures with relatively low free energy [10] but only two were observed experimentally [3,20]. Usually the so-called radial spherical structure (Frank-Pryce model [21]) is observed in the absence of the electric field. This structure has a single $s=2$ χ line that extends from the center to the droplet surface. A low electric field does not result in struc-

tural changes of the director field, but the radial defect line tilts into position normal to the field [3,9]. The other observed structure is the so-called diametrical structure with a single $s=1$ χ line which extends from one pole to the other. In low electric field the defect line tends to be either parallel (stable orientation) or perpendicular (metastable orientation) to the applied field.

This gives three experimentally possible initial spherical structures, stabilized by the low electric field. Each of them evolves in its own way, giving three intermediate oblate structures. The structures are named after the position of the defect lines with respect to the applied electric field and after the spherical structure they originate from. Detailed mathematical description of director fields of intermediate structures is given in the Appendix.

1. Parallel diametrical oblate structure

This structure appears when the diametrical spherical structure is in its stable position in low electric field. In high enough field the central circle with a bipolar structure is created and the $s=1$ χ line splits into two $s=\frac{1}{2}$ χ lines which remain parallel to the applied field. Each defect line penetrates the central circle in an $s=\frac{1}{2}$ point defect, characteristic for the two-dimensional bipolar structure that builds up on the central circle [Fig. 3(a)].

Construction of the director field in *the parallel diametrical oblate* (PDO) structure is the simplest one. It is obtained by the first method, described in the Sec. II B 1. According to the bipolar structure on the central circle the distance between the two defect lines equals 2δ and they lie symmetrically with respect to the center of the droplet. With increasing δ they get shorter and shorter and finally disappear on the droplet surface for $\delta \geqslant R$. Length of each line is $2\sqrt{R^2-\delta^2}$. There are no surface defect lines as in the previous model, because of the finite anchoring strength.

2. Normal diametrical oblate structure

If the initial orientation of the diametrical χ line is perpendicular to the field, the line breaks in two parts separated with the central circle of radius δ. The two lines are naturally still perpendicular to the applied field. Let this structure be called *normal diametrical oblate* (NDO) structure. (A better name would probably be perpendicular diametrical oblate structure, but this would lead to the abbreviation PDO, which is the same as for the parallel diametrical oblate structure.)

Since the defect lines in this structure are in the plane of the central circle the second method must be used to construct the director field in the droplet (see Fig. 4). The structure on the central circle is again bipolar and $s=1$ χ lines lie symmetrically with respect to the droplet center. Each line has length $R-\delta$ and disappears on the droplet surface when $\delta \geqslant R$.

The normal and parallel diametrical oblate structure are somewhat similar although this is not obvious at first glance. Nevertheless, one structure can be continuously transformed into the other by the procedure of stretching, described in the Sec. II B 1. Let us start with a parallel structure. The points where defect lines are attached to the central circle are kept fixed, but the ''upper'' and the ''lower'' half of the $s=\frac{1}{2}$ χ defect line are rotated into the plane of the central circle (see Fig. 4). Then both halves of the $s=\frac{1}{2}$ χ line fuse, the $s=1$ χ line appears, and the normal diametrical oblate structure shows up. The described topological transformation confirms the similarity between the two structures, but energy considerations are required to determine whether or not such a transition is really possible.

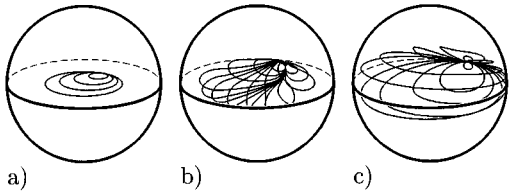

FIG. 6. Schematic three-dimensional presentation of the director field in the NRO structure for $\delta=R/2$ and $qR=2\pi$. Several chiral nematic surfaces are shown: (a) the central circle, (b) the N^* surface with $d=R/4$, and (c) the N^* surface with $d=R/2$. The corresponding angles of rotation of the director are $0,\pi/2$, and π, respectively.

3. Normal radial oblate structure

The third oblate structure originates from the initial radial spherical structure. In low fields the $s=2$ χ line is stable when it is normal to the applied electric field. When the field increases sufficiently, the central circle with monopolar director field is created [see Fig. 3(b)] and the former radial defect line is attached to its border. Because of the normal defect line let this structure be called *the normal radial oblate* (NRO) structure. As in the case of the normal diametrical oblate structure, the second method is used to construct the director field in the droplet. The characteristic χ line with strength $s=2$ has length $R-\delta$ and disappears at the droplet surface when $\delta \geqslant R$. A schematic presentation of the director field for this structure is given in Fig. 6.

III. TRANSITION

To obtain the stability diagrams of the structures their free energy has to be determined. Since the model director fields are known the free energy is in principle easy to calculate. The bulk part is an integration of the bulk free energy density, whereas the surface contribution is a surface integral of the surface free energy density. There are, however, some numerical difficulties, related to a relatively time consuming computation. The total free energy is obtained in the following way.

The surface contribution results from a nonparallel alignment of the director at the droplet surface, as described in Sec. II A. The surface free energy [Eq. (2)] is rewritten as

$$\frac{W_0}{2} \oint_S \left(\vec{n}(\vec{R}) \cdot \frac{\vec{R}}{R} \right)^2 dS. \tag{8}$$

The bulk contribution is composed of two parts, an elastic part due to deformed director field in the droplet and a field part due to dielectric anisotropy of the N^* phase. The elastic free energy density has the usual Frank form

$$f_{\text{elastic}}=\frac{K_{11}}{2}(\vec{\nabla}\cdot\vec{n})^2+\frac{K_{22}}{2}[q+\vec{n}\cdot(\vec{\nabla}\times\vec{n})]^2 + \frac{K_{33}}{2}|\vec{n}\times(\vec{\nabla}\times\vec{n})|^2 - \frac{K_{24}}{2}\vec{\nabla}\cdot[\vec{n}\times(\vec{\nabla}\times\vec{n})+\vec{n}(\vec{\nabla}\cdot\vec{n})], \quad (9)$$

where K_{11}, K_{22}, K_{33}, and K_{24} are the splay, twist, bend, and saddle-splay elastic constants, respectively, and $q=2\pi/\mathcal{P}$ is the intrinsic wave number of the N^* phase. The saddle-splay free energy contribution is zero for all spherical and planar structures and relatively small when compared to the splay and bend contribution for oblate structures. Therefore it is not included in the forthcoming calculations. Assuming that the electric field inside the droplet is equal to the applied electric field, the field free energy density is

$$f_{\text{field}}=-\tfrac{1}{2}\varepsilon_0\varepsilon_a(\vec{n}\cdot\vec{E})^2, \quad (10)$$

where $\varepsilon_a=\varepsilon_\parallel-\varepsilon_\perp$ is the dielectric anisotropy of the N^* phase. Assumption of homogeneous electric field may be a very crude estimate, as the director field varies considerably over droplets. And even if the assumption of homogeneous field inside the droplet is acceptable, the field inside the droplet is not necessarily equal to the applied one. Since the droplets are confined to a polymer matrix, which does not have to have the same average dielectric constant as the N^* phase, the field in the droplet is connected with the field in the polymer matrix. As an estimate, the droplet in the matrix can be considered as a uniform sphere with dielectric constant equal to the average dielectric constant of the N^* phase $\overline{\varepsilon}$. If it is further assumed that the conductivities of the polymer matrix and liquid crystal are negligible, that the droplets are not very close to each other—this is opposite to the requirements of the applications [5]—and that the electrodes are far enough apart, the electric field in the droplet is approximately equal,

$$E'\approx\frac{3}{\kappa+2}E, \quad \kappa\equiv\frac{\overline{\varepsilon}}{\varepsilon_{\text{PM}}}, \quad (11)$$

where E' is the field in the droplet, E the field in the polymer matrix away from the droplet, and ε_{PM} is the dielectric constant of the polymer matrix. If both dielectric constants are approximately equal ($\kappa=1$) the electric field in the droplet can be taken equal to the applied electric field. This further means that the field in the droplets is not affected by the neighboring droplets, since the field in the matrix is not changed. Otherwise the electric field E that enters the free energy expressions must be replaced by E'. On the other hand, if the conductivity of the polymer matrix and liquid crystal is not negligible, the electric field in the droplet is approximately related to the applied low frequency electric field as

$$E'\approx\frac{3}{\tilde{\kappa}+2}E, \quad \tilde{\kappa}\equiv\frac{\overline{\sigma}}{\sigma_{\text{PM}}}, \quad (12)$$

where $\overline{\sigma}$ is the average conductivity of liquid crystal and σ_{PM} is the conductivity of polymer matrix [22].

The integration of the free energy density is performed numerically. There are no problems with the surface, field, and twist contributions, but bend and splay free energy densities diverge in the vicinity of χ lines. The isotropic cores of defects are introduced to overcome this difficulty, but the numerical integration remains quite problematic because of the rapid changes of the free energy in the vicinity of these cores. Therefore an iterative integration method is used. The starting mesh of points used for integration is given, but in the regions of rapidly changing free energy new mesh points are added in order to reduce the influence of each mesh point. This is the most important advantage of the analytical form of the director field and free energy density. The free energy is calculated for the values of parameter ϵ in the interval from 0 to 1. Calculated contributions (bend, field, and surface) are then expressed with appropriate analytical functions that fit numerically obtained values the best.

Each contribution to the free energy can be separated into two parts. The first one describes the average behavior of the function while the other one, which is smaller than the first one, reflects the periodic structure in the droplets. The latter one is sinelike modulated with a wave number $2q$, where the factor 2 is a consequence of the head-tail symmetry of the nematic phase. The core and twist contributions to the free energy do not have the modulated part, and the influence of the modulated part on the surface free energy is negligible, compared to the average behavior and numerical uncertainty of the results. On the other hand, modulations of the splay, bend, and field free energy are clearly visible and not negligible—the relative amplitude of oscillations is up to 10%. For all three contributions the amplitude of the sinelike modulation becomes smaller with increasing ϵ. As expected, another important feature is that the modulation gets smaller with increasing chirality, i.e., with increasing q. Hereafter the one elastic constant approximation is employed, because the splay and bend contribution add to a nonmodulated function when the corresponding elastic constants are set equal ($K_{11}=K_{33}$). Only the field free energy is described with both average and modulated functions. This makes the calculations as simple as possible, but on the other hand the description is complete enough to explain the steplike behavior of the transition.

In order to quantify the sinelike modulation, the field contribution is first described with a polynomial function, which describes the average dependence on ϵ. Next the optimal polynomial function is subtracted from the numerically calculated field free energies and the difference is approximately described with a function of the form $A(\epsilon)\sin(2qR\epsilon)$, where amplitude $A(\epsilon)$ is again polynomial. The error, obtained when subtracting two large, almost equal numbers, which carry their own (in this case numerical) error is known to be large. For example, if the amplitude of the modulation is as much as 5% of the optimal polynomial function, then the relative errors, made by subtraction, are more than 20 times larger than the numerical errors, made by numerical integration. Therefore the amplitude $A(\epsilon)$ is derived with a considerably larger uncertainty than the polynomial that describes the average behavior of the field free energy contribution. That is why the steplike behavior of the

TABLE I. Fitted free energies in the high chirality limit ($qR=60\pi$) and one elastic constant approximation: $K_{11}=K_{22}=K_{33}\equiv K=5\times10^{-12}$ N. The radius of the droplet equals $R=10$ μm and the dielectric anisotropy equals $\varepsilon_a=-5$. All free energies are given in the units πKR. The electric field is normalized with respect to the electric field E_0, which results in an electric coherence length that is equal to the droplet radius $\xi_E(E_0)=R$, $E_0=0.0336$ V/μm. Since the surface and field free energies of the three structures are equal within numerical error, only two analytical functions are needed to describe the surface and field free energy contributions for all three structures.

Contribution	Free energy (units of πKR)
Elastic: PDO	$13.01+10.58\epsilon-3.608\epsilon^2-7.983\epsilon^3-9.155e^{30(\epsilon-1)}+1.178e^{-400\epsilon}$
Elastic: NDO	$14.993-6.372\epsilon+5.0285\epsilon^2-6.1055\epsilon^3-6.614e^{35(\epsilon-1)}$
Elastic: NRO	$27.178-16.291\epsilon+13.305\epsilon^2-12.860\epsilon^3-8.17e^{28(\epsilon-1)}$
Field	$(0.221\,34-0.1788\epsilon-0.273\epsilon^2+0.229\epsilon^3)\times(E/E_0)^2$
Surface	$\epsilon^2(0.3194\epsilon+0.3555)\times(RW_0/K)$

transition should not be taken too quantitatively. There is clearly a steplike transition in question, but whether a particular step occurs at slightly higher or lower electric field is beyond the accuracy of the calculations presented here.

The resulting analytical functions are used to write down the expression for the total free energy of the particular oblate structure as a function $\mathcal{F}(\epsilon,E)$. To predict a physically meaningful state, the free energy must be minimized for given electric field E. Therefore the derivative $\partial\mathcal{F}/\partial\epsilon$ must be zero. This yields a relation $\epsilon(E)$, but for practical reasons the inverse function $E(\epsilon)$ is calculated. Once this function is known, the total free energy for a particular oblate structure can be compared with the free energy of the corresponding spherical structure to obtain the stability diagram. The total free energy of spherical structures can be obtained by setting $\epsilon=0$ in the expressions for the oblate structures. In addition, it can be obtained analytically for equal elastic constants. For illustration of the above reasoning the parts of the analytical function $\mathcal{F}$ that describe particular contributions to the free energy for the case $qR=60\pi$ are written in Table I. Note that there is no modulated part in the expression for the field free energy. This is a consequence of high chirality: the amplitude of the modulated part is smaller than the numerical accuracy.

IV. RESULTS

In this section the above described procedures are used to describe in detail the field induced transition in chiral nematic droplets. First, in the high chirality limit ($qR=60\pi$), transitions via all three intermediate structures are compared. The amplitude of the field free energy sinelike modulation is here so small that steplike behavior is no longer visible (see Fig. 7). The threshold values for all three structures, as well as the growth of the central region as a function of the field are similar, but in detail the behavior of the PDO structure is qualitatively different from the behavior of the other two structures. Free energy calculations show that the PDO structure with a small nonzero $\epsilon(\sim0.009)$ has lower free energy than the corresponding spherical structure even at zero electric field. Nevertheless, the growth of ϵ starts at approximately the same threshold electric field for all three structures.

Next the influence of chirality is studied. In Fig. 8 the transition for each intermediate structure is drawn for $qR=60\pi$, 20π, and 10π. The overall behavior does not change much for the three chiralities, but there is a qualitative change due to sinelike modulation of the field contribution to the free energy, which is more pronounced for smaller q.

Finally, the influence of surface anchoring is studied (see Fig. 9). With stronger surface anchoring the threshold field increases and the transition is completed at a higher field. Such a behavior is expected, since the transition is mainly governed by the competition between surface and field effects, whereas the bulk elasticity is important only at the beginning of the transition. For example, the anchoring strength $W_0=2\times10^{-4}$ J/m^2 (see [14]) makes the maximal surface contribution, which is reached in planar structures, equal to approximately $270\pi KR$. On the other hand, maximal elastic free energy is realized in spherical structures, in particular, in the radial spherical structure [9,10], where it equals approximately $27\pi KR$. It is instructive to realize that the electric field contribution for $\varepsilon_a=-5$ and $E=1$ V/μm would equal approximately $200\pi KR$ for spherical structures, if they were still stable.

As stated above, the balance between electric and surface forces mainly governs the structural transition. Therefore the

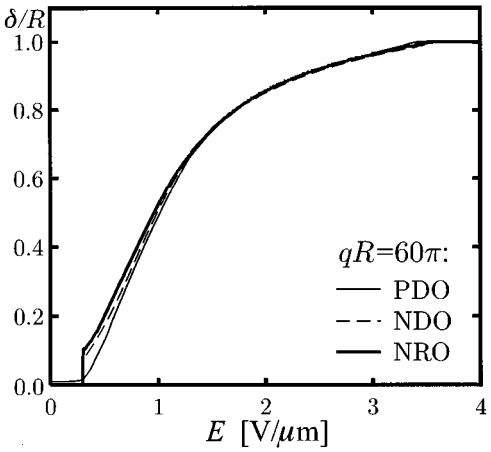

FIG. 7. Comparison of the transition for three possible intermediate structures: parallel diametrical oblate, normal diametrical oblate, and normal radial oblate structure. The behavior of the three differs mostly at the beginning of the transition, whereas $\epsilon\equiv\delta/R$ behaves similarly for all three at intermediate electric fields.

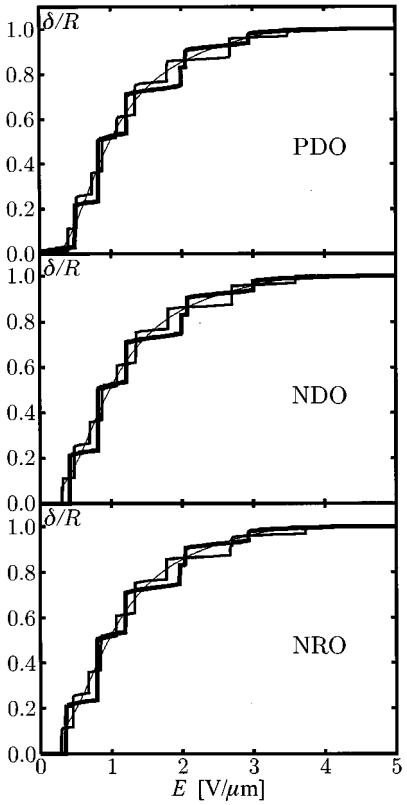

FIG. 8. Upper diagram shows the transition curve for the planar diametrical oblate structure, the middle that one for the normal diametrical oblate structure, and the lower one that for the normal radial oblate structure. On each diagram the curves for three different chiralities are shown: $qR=10\pi$ (the thickest line), $qR=20\pi$ (line of medium thickness), and $qR=60\pi$ (the thinnest line). For the highest chirality ($qR=60\pi$) the sinelike modulation of the field free energy is too small to make a reliable fit. Therefore the transition curve is smooth. For all three structures the transition curves do not move due to different chiralities, but their shape changes—the steplike behavior is a direct consequence of the sinelike modulation of the field free energy contribution and is more pronounced for smaller chiralities.

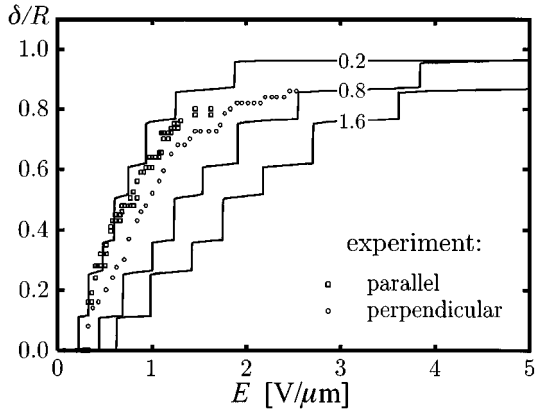

FIG. 9. Influence of the anchoring strength is presented. Theoretical curves are calculated in the one elastic constant approximation: $qR=20\pi$, $R=10$ μm, $\epsilon_a=-5$, $K=5\times10^{-12}$ N. The anchoring strength is written on each curve in mJ/m^2. A comparison with the experimental observations parallel (squares) and perpendicular (circles) to the field, made by Kitzerow and Crooker [3], indicates that the anchoring strength should be $W_0=0.2$–0.4 mJ/m^2.

shape of the transition function $\epsilon(E)$ depends not only on the anchoring strength W_0 (see Fig. 9), but also on the dielectric constants of N^* phase and polymer matrix. The corresponding parameter is proportional to the ratio between the surface and field free energy: $\kappa=1$ this means $W_0/(R|\varepsilon_a|)$. The radius of the droplet enters the expression due to the fact that the surface contribution is proportional to R^2 and the field contribution to R^3.

A general remark about the limitations of the derived free energies and resulting transitions should be made at this point. There are two reasons for limitations: the first is due to the model itself, the other is a consequence of numerical calculations.

(a) Numerical precision is not critical for the surface and field free energies as their densities change very smoothly without sharp peaks. A starting three-dimensional mash of approximately $100\times100\times100$ points results in an error smaller than 0.1%. Problems arise when the elastic free energy density, which has singularities in the vicinity of the defect lines, is integrated. In order to calculate the free energy in a reasonable amount of time the accuracy is limited to 1%.

(b) Model limitations are most pronounced for small ϵ's, especially for both normal oblate structures, because of our procedure, where the director field in the entire droplet is obtained from the director field on the central circle. First of all, the deformations on a circle with a radius δ close to the core radius are strong and the variations of the scalar order parameter should be included in the calculations of director field [23]. Second, for a small δ the stretching factor [Eq. (7)] is much greater than 1. As a consequence, any discrepancy between the actual and modeled director field on a central circle will result in a much larger discrepancy in the rest of the droplet. In the limit $\epsilon\rightarrow0$ the stretching factor diverges, indicating that modeled director fields for small ϵ's are not reliable. Indeed, the numerically integrated elastic free energies of both normal structures for $\epsilon=0$ are about 6% larger than the analytically obtained ones. This simply means that models for normal oblate structures do not transform into corresponding spherical structures for $\epsilon=0$, although the small difference in free energies shows that the discrepancy is not large. On the other hand, for equal elastic constants, the elastic free energy density of the $\epsilon=0$ PDO structure transforms into the free energy of the diametrical spherical structure [10], confirming that the two structures are really the same. The other limitation of the model shows up at the end of the transition. When $\epsilon=1$ all N^* surfaces are parallel and the electric free energy is zero. Therefore the director field in the droplet depends on the competition between surface and bulk elastic forces alone, but there are no topological constraints, because there are no closed N^* surfaces. The model is, however, based on closed N^* surfaces, so the final planar structures are not described adequately. Therefore it is possible that the transition is not continuous at the end. The conclusion of the above considerations is the following. Transitional structures are optimally modeled for parameters ϵ in the middle of the interval [0,1], whereas at the limits of the interval, in particular for small ϵ, the models are less reliable.

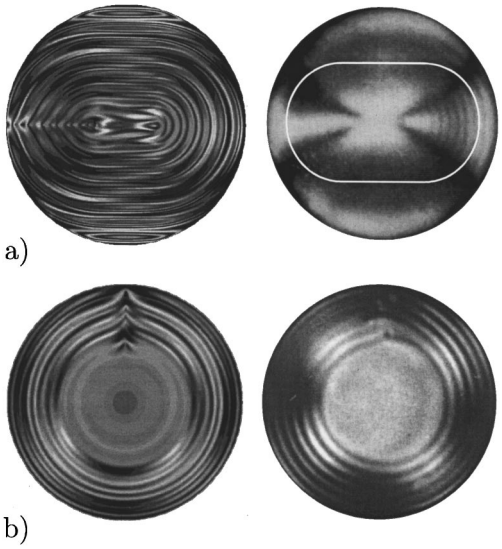

FIG. 10. Simulated textures (left) are compared with the experimental ones (right). In the upper figure (a) the droplets are observed in the direction perpendicular to the applied electric field $\vec{E}$ [compare with Figs. 2(b) and 2(c)]. One chiral nematic surface is drawn in the experimental micrograph to ''guide the eye.'' In the lower figure (b) the viewing direction is parallel to the applied electric field. A flat central region is clearly seen: its radius δ is about one-quarter of the droplet radius R in the upper figure and one-half of the droplet radius R in the lower figure.

In order to verify the structures form another point of view, simulations of the polarizing microscope textures are compared with the textures observed by Kitzerow and Crooker [3]. An example for normal radial oblate structure with $\epsilon \sim 0.5$ is presented in Fig. 10. The simulations are based only on polarization rotations and phase shifts, whereas the diffraction effects at the droplet surface are ignored because the studied droplets are large enough. In order to simulate a black and white photograph textures for different wavelengths are weighted and combined into a single gray scale figure. The combination corresponding to the relative sensitivity of the photographic film is [24] 470 nm, 20%; 535 nm, 60%; and 600 nm, 20%. For a detailed description of the calculation of light transmission and textures in liquid crystals see [24,25]. The simulated textures show excellent agreement with experiments and confirm that our calculations are correct within the framework of the limitations described above. The distance between successive dark or light fringes in Fig. 10(b) is approximately one-half of the pitch.

V. SUMMARY

In this paper, continuous structural transitions in a spherical chiral nematic droplet under the influence of an electric field are studied theoretically. In particular, the intermediate structures are modeled with oblate chiral nematic surfaces that enable a continuous transition from low-field spherical to high-field planar structures (see Figs. 2 and 10). Further, analytical expressions for director fields of intermediate structures are developed (see Figs. 4 and 6 and the Appendix). The procedure is based on the known director field on the central circle and chiral character of the liquid crystal. The analytical director fields developed here and the resulting evolution of the transition with applied electric field are in reasonable qualitative and quantitative agreement with the experimental data [3]. It is proved that the transition is mainly governed by field and surface forces. In other words, the threshold electric field as well as the evolution of the intermediate oblate structures are characterized by the parameter $W_0/(R|\varepsilon_a|)$. This gives an opportunity to determine either dielectric anisotropy ε_a or anchoring strength W_0, if the other is known. For example, assuming $\varepsilon_a = -5$, $K = 5 \times 10^{-12}$ N, and $R = 10$ μm, the anchoring strength is estimated to be $W_0 = 0.2 - 0.4$ mJ/m^2 (see Fig. 9). The observed steplike behavior can be qualitatively explained using a model with sinelike modulation of the electric part of the free energy, which is related to the periodicity of structures in chiral nematic phase.

Although the calculations are performed in the one elastic constant approximation, generalization to the nonequal elastic constant and inclusion of the saddle-splay (K_{24}) term is possible even with the very same model, as long as the splay (K_{11}) and bend (K_{33}) elastic constants are not too different from each other. That limitation is a result of the construction of the director fields, which originate from a director field on the central circle that is calculated for equal elastic constants (see the Appendix). Strong variations of the ratio between bend and splay elastic constants, such as K_{33} divergence on approaching the nematic-smectic transition, would certainly require a different form of the director field on the central circle.

The electric field inside the droplet is treated as homogeneous, which might be a crude estimate, but good agreement with the experiments confirms that possible nonhomogeneities do not influence the transition significantly. Nevertheless, the change of the electric field strength in the droplet due to mismatching of dielectric constants of polymer matrix and liquid crystal is taken into account.

Finally, it should be mentioned that in real systems, the radial structures occur much more frequently than the diametrical ones [3,20]. On the other hand, the above calculations show (see Fig. 5) that the elastic free energy of the radial structures is approximately twice as large as the elastic free energy of the diametrical structures. This discrepancy between experimental observations and theoretical predictions remains to be explained.

ACKNOWLEDGMENTS

Financial support from the Ministry of Science and Technology of Slovenia (Grant No. J2-7067) and the European Union (Project No. CIPA-CT93-0159) is gratefully acknowledged. The experimental pictures in Fig. 10, similar to those in [3], were kindly provided by Peter Crooker.

APPENDIX: DIRECTOR FIELDS

As described above, the director field in a droplet is determined by the director field on the central circle of radius δ (Fig. 3) and one of the described procedures which corresponds to defect lines parallel or perpendicular to the applied electric field. In this section the director fields for all three

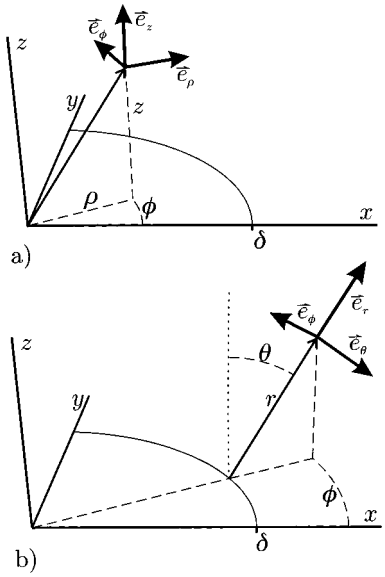

FIG. 11. Coordinate systems used to write down the director field in the droplet: (a) cylindrical coordinate system for the flat region ($x^2+y^2\leq\delta^2$) and (b) toroidal coordinate system for the curved region of the droplet ($x^2+y^2>\delta$). The radius δ of the flat central region is drawn in the xy plane.

studied oblate structures are calculated. In order to present the director field as clearly as possible appropriate coordinate systems are chosen: cylindrical (ρ,ϕ,z) for the flat central region of the droplet and toroidal (r,θ,ϕ) for the rest of the droplet (see Fig. 11).

1. Central circle

The two-dimensional director field on the central circle is determined by the infinitely strong parallel anchoring at the circle border due to the λ defect line at the border. This λ line is a direct topological consequence of the shape of the N^* surfaces and is therefore unavoidable. Therefore the anchoring at the border of the circle is infinitely strong and also the sum of the defects' strength on the circle equals 1. Two possible director fields on the circle are of interest.

The bipolar director field has two point defects of equal strength, lying diametrically opposite to each other [see Fig. 3(a)]. Any point defect at the border of a two-dimensional nematic can be treated topologically as an interior (bulk) or border (surface) defect. The distinction between the two descriptions is that if a defect is surfacelike, only one-half of it is actually inside the nematic phase. That is why the director field of a defect with the interior strength s, pushed to the border, looks like the director field of a bulk defect with the strength $s'=2s$. As the sum of the bulk strengths of the defects on the circle equals 1, the bipolar director field is characterized by two surface defects with strength $s'=1$ or equivalently two bulk defects with strength $s=\frac{1}{2}$. As far as a mathematical representation of the director field is concerned there is no difference between the two descriptions. In the cylindrical coordinate system the director field of the bipolar structure reads

$$\vec{n}=\frac{(\delta^2-\rho^2)\sin\phi}{\sqrt{\delta^4+\rho^4+2\delta^2\rho^2\cos(2\phi)}}\vec{e}_\rho + \frac{(\delta^2+\rho^2)\cos\phi}{\sqrt{\delta^4+\rho^4+2\delta^2\rho^2\cos(2\phi)}}\vec{e}_\phi. \tag{A1}$$

This director field is an exact solution for equal elastic constants and was obtained, for example, in [14].

The monopolar director field has one point defect ($s'=2$) at the border of the circle. In this case the director field is obtained from the known solution for the bulk case $s=2$ and equal elastic constants. In an unconstrained two-dimensional nematic the director field near the $s=2$ point defect can be represented as a family of circles with one common point. If this point is placed at the border of the central circle and the entire director field is rotated so that one of the director field's circles coincides with the border of the central circle, the monopolar director field shows up [see Fig. 3(b)]. The director field in cylindrical coordinates reads

$$\vec{n}=\frac{(\rho^2-\delta^2)\cos(\phi)}{\delta^2+\rho^2-2\delta\rho\,\sin\phi}\vec{e}_\rho+\frac{(\rho^2+\delta^2)\sin\phi-2\delta\rho}{\delta^2+\rho^2-2\delta\rho\,\sin\phi}\vec{e}_\phi. \tag{A2}$$

2. Oblate chiral nematic surfaces

The director field at a particular point B on the N^* surface is obtained by appropriate rotation of the director at point A on the central circle [see Fig. 2(b)]. In the director fields of normal oblate structures (NDO and NRO), stretching of the director field is necessary to get defect lines in the plane of the central circle. Note that in the flat region the director does not have a z component and that in the curved region the director does not have an r component (in toroidal coordinates). This is a natural consequence of the shape of the N^* surfaces. Note further that the director field on closed and cutoff N^* surfaces is obtained with the same procedure because the director field is not altered in the vicinity of the droplet surface.

The parallel diametrical oblate structure is the simplest one, since no stretching is needed. The director field in the flat region is obtained by a rotation of the bipolar director field on the central circle,

$$\vec{n}=\frac{\sin(\phi-qz)-\varrho_P^2\sin(\phi+qz)}{\sqrt{1+\varrho_P^4+2\varrho_P^2\cos2\phi)}}\vec{e}_\rho + \frac{\cos(\phi-qz)+\varrho_P^2\cos(\phi+qz)}{\sqrt{1+\varrho_P^4+2\varrho_P^2\cos(2\phi)}}\vec{e}_\phi, \tag{A3}$$

where $\varrho_P=\rho/\delta$ is a dimensionless radial cylindrical coordinate, normalized with respect to the radius δ of the central circle. The index P stands for ''parallel.'' The χ lines with bulk strength $s=\frac{1}{2}$ consist of the points $\{(\rho=\delta,z,\phi=\pm\pi/2)\}$ and are parallel to the z axis, i.e., the direction of the applied field. The director field in the curved region is even simpler,

$$\vec{n} = -\sin(qr)\vec{e}_\theta + \cos(qr)\vec{e}_\phi, \tag{A4}$$

and obviously does not have any defects.

The normal diametrical oblate structure originates from a bipolar structure on the central circle, similar to the PDO structure, but here the defect lines lie in the plain of the central circle, i.e., normal to the applied electric field. The director field at point B does not originate from the same point A on the central circle as for the PDO structure [see Fig. 2(b)], but from a point closer to the circle center due to the stretching [see Eq. (7) and Fig. 4], involved in the construction of the director field. The result in the central region is

$$\vec{n} = \frac{\sin(\phi - qz) - \varrho_N^2 \sin(\phi + qz)}{\sqrt{1 + \varrho_N^4 + 2\varrho_N^2 \cos(2\phi)}}\,\vec{e}_\rho + \frac{\cos(\phi - qz) + \varrho_N^2 \cos(\phi + qz)}{\sqrt{1 + \varrho_N^4 + 2\varrho_N^2 \cos(2\phi)}}\,\vec{e}_\phi, \tag{A5}$$

where $\varrho_N \equiv \rho\,\eta(z)/\delta$ is a stretched dimensionless radial cylindrical coordinate, normalized with respect to the radius δ of the central circle. The index N stands for ''normal'' and $\eta(z) \equiv 2e/(2e + \pi|z|)$ is the corresponding stretching factor in the flat central region. In the outer region the director field, written in toroidal coordinates, reads

$$\vec{n} = \frac{\sin(\phi - qr) - \eta^2(r,\theta)\sin(\phi + qr)}{\sqrt{1 + \eta^4(r,\theta) + 2\eta^2(r,\theta)\cos(2\phi)}}\,\vec{e}_\theta + \frac{\cos(\phi - qr) + \eta^2(r,\theta)\cos(\phi + qr)}{\sqrt{1 + \eta^4(r,\theta) + 2\eta^2(r,\theta)\cos(2\phi)}}\,\vec{e}_\phi, \tag{A6}$$

where $\eta(r,\theta) \equiv (2e + 2r\theta)/(2e + \pi r)$ is the corresponding stretching factor in the curved region of the droplet. Note that η is chosen in such a way that it equals 1 for $\theta = \pi/2$, i.e., the director field at the border of the central circle is used as the origin of the director field in the equatorial plane of the outer region of the droplet with the curved N^* surfaces. The χ lines with bulk strength $s = 1$ can be represented as the points $\{(r, \theta = \pi/2, \phi = \pm\pi/2)\}$.

The normal radial oblate structure is obtained from the monopolar director field on the central circle with the procedure analogous to the one used for the NDO structure. In the central region the resulting director field in cylindrical coordinates reads

$$\vec{n} = \frac{\varrho_N^2 \cos(\phi + qz) - \cos(\phi - qz) + 2\varrho_N \sin(qz)}{1 + \varrho_N^2 - 2\varrho_N \sin\phi}\,\vec{e}_\rho + \frac{\varrho_N^2 \sin(\phi + qz) + \sin(\phi - qz) - 2\varrho_N \cos(qz)}{1 + \varrho_N^2 - 2\varrho_N \sin\phi}\,\vec{e}_\phi, \tag{A7}$$

where the abbreviation ϱ_N was introduced in the preceding paragraph. For the curved region the director field is

$$\vec{n} = \frac{\eta^2(r,\theta)\cos(\phi + qz) - \cos(\phi - qz) + 2\,\eta(r,\theta)\sin(qz)}{1 + \eta^2(r,\theta) - 2\,\eta(r,\theta)\sin\phi}\,\vec{e}_\theta + \frac{\eta^2(r,\theta)\sin(\phi + qz) + \sin(\phi - qz) - 2\,\eta(r,\theta)\cos(qz)}{1 + \eta^2(r,\theta) - 2\,\eta(r,\theta)\sin\phi}\,\vec{e}_\phi, \tag{A8}$$

where $\eta(r,\theta)$ was again introduced in the preceding paragraph.

The comparison between the director field in the flat (cylindrical) and curved (toroidal) region of the droplet reflects the procedure that was used in the construction of the director field. Let us briefly summarize the procedure. The toroidal part of the director field of both normal oblate structures (NDO and NRO) is obtained from the director field in the flat part of the droplet by the following substitutions: the variable ϱ_N is replaced by $\eta(r,\theta)$, the cylindrical z component of the director becomes the toroidal r component of the director, the cylindrical ϕ component of the director becomes the toroidal ϕ component of the director, the cylindrical ρ component of the director becomes the toroidal θ component of the director, and the cylindrical coordinate z is replaced by the toroidal coordinate r.

[1] D. K. Yang and P. P. Crooker, Liq. Cryst. **9**, 245 (1991).
[2] H.-S. Kitzerow and P. P. Crooker, Liq. Cryst. **11**, 561 (1992).
[3] H.-S. Kitzerow and P. P. Crooker, Liq. Cryst. **13**, 31 (1993).
[4] P. P. Crooker, H.-S. Kitzerow, and F. Xu, Proc. SPIE **2175**, 173 (1994).
[5] H.-S. Kitzerow, Liq. Cryst. **16**, 1 (1994).
[6] J. W. Doane, in *Liquid Crystals—Applications and Uses*, edited by B. Bahadur (World Scientific, Singapore, 1990), Vol. 1, p. 361.

[7] D. K. Yang, J. W. Doane, Z. Yaniv, and J. Glasser, Appl. Phys. Lett. **64**, 1905 (1994).
[8] P. G. de Gennes and J. Prost, *The Physics of Liquid Crystals* (Clarendon, Oxford, 1996).
[9] J. Bajc, J. Bezić, and S. Žumer, Phys. Rev. E **51**, 2176 (1995).
[10] J. Bezić and S. Žumer, Liq. Cryst. **11**, 593 (1992).
[11] S. Žumer, S. Kralj, and J. Bezić, Mol. Cryst. Liq. Cryst. **212**, 163 (1992).
[12] A. Rapini and M. Papoular, J. Phys. (Paris) Colloq. **30**, C4-54 (1969).
[13] D. W. Allender, G. P. Crawford, and J. W. Doane, Phys. Rev. Lett. **67**, 1442 (1991).
[14] G. P. Crawford, D. W. Allender, and J. W. Doane, Phys. Rev. A **45**, 8693 (1992).
[15] R. J. Ondris-Crawford, M. Ambrožič, J. W. Doane, and S. Žumer, Phys. Rev. E **50**, 4773 (1994).
[16] J. Bezić and S. Žumer, Liq. Cryst. **14**, 1695 (1993).
[17] M. Ambrožič and S. Žumer, Phys. Rev. E **54**, 5187 (1996).
[18] H.-S. Kitzerow, B. Liu, F. Xu, and P. P. Crooker, Phys. Rev. E **54**, 568 (1996).
[19] A. Kilian and A. Sonnet, Z. Naturforsch. Teil A **50**, 991 (1995).
[20] Y. Bouligand and F. Livolant, J. Phys. (Paris) **45**, 1899 (1984).
[21] J. R. Quigley and W. J. Benton, Mol. Cryst. Liq. Cryst. **42**, 43 (1977).
[22] J. Erdmann, J. W. Doane, S. Žumer, and G. Chidichimo, Proc. SPIE **1080**, 32 (1989).
[23] S. Kralj, S. Žumer, and D. W. Allender, Phys. Rev. A **43**, 2943 (1991).
[24] R. J. Ondris-Crawford, E. P. Boyko, B. G. Wagner, J. H. Erdmann, S. Žumer, and J. W. Doane, J. Appl. Phys. **69**, 6380 (1991).
[25] A. Scharkowski, G. P. Crawford, S. Žumer, and J. W. Doane, J. Appl. Phys. **73**, 7280 (1993).